Inorg. Chem. **2007**, *46*, 7351–7361

Metalloporphyrin-Based Inclusion Materials: Exploiting Ligating Topologies and Hydrogen-Bonding Backbones in Generating New Supramolecular Architectures

D. Krishna Kumar,[†] Amitava Das,*[,†] and Parthasarathi Dastidar*[,‡]

Department of Organic Chemistrty, Indian Association for the Cultivation of Science, 2A&2B Raja S. C. Mullick Road, Jadavpur, Kolkata-700032, West Bengal, India, and Analytical Science Discipline, Central Salt & Marine Chemicals Research Institute (CSIR), G. B. Marg, Bhavnagar-364 002, Gujarat, India

Received February 5, 2007

By coordination of the metal center of tetraphenylmetalloporphyrins (TPMP) [metal center = Zn(II) or Mn(II)] with pyridyl-based bidentate ligands, namely, *N*,*N*′-bis(4-pyridyl)urea (4BPU), *N*,*N*′-bis(3-pyridyl)urea (3BPU), and *N*-(4-pyridyl)isonicotinamide (4PIN), various axially modified tetraarylmetalloporphyrins (AMTAMPs) have been crystallographically characterized in their corresponding lattice inclusion complexes. Nine such inclusion crystals are prepared by crystallizing TPMP and the corresponding bidentate ligands in 1:2 molar ratio from suitable solvent systems. While the metal center Zn(II) of TPMP leads to the formation of both dimeric and monomeric AMTAMPs due to its preference for pentacoordinated geometry, the Mn(II) metal center of TPMP forms both polymeric and discrete hexacoordinated AMTAMPs due to its preference for hexacoordinated geometry. However, there seem to be no control on the formation of a particular AMTAMP. Structural analyses suggest that most of the AMTAMPs display new types of packing in the corresponding inclusion crystals.

Introduction

Molecules/building blocks that are unable to pack efficiently in all the three dimensions tend to form supramolecular architecture with voids, open channels that are filled with guest molecules during crystal formation resulting in lattice inclusion materials;[1] these are important materials because of their several applications that include conversion of liquids to solids, molecular separation, controlled release of guests, and supramolecular storage of reagents. The key to the design of a lattice inclusion host lies in the judicial choice of the building block that would self-assemble primarily via nonbonded interactions generating a supramolecular architecture with voids and/or channels within which the guest molecules are occluded. The foremost characteristic of a good building block is its rigidity. Tetraarylporphyrins (TAPs) and tetraarylmetalloporphyrins (TAMPs) being conjugated symmetrical macrocycles possess high rigidity and high molecular symmetry that are essential for the design of good building blocks.[2] Moreover, they are relatively easily synthesized and chemically modified, thermally stable, and largely unreactive; all these qualities are conducive for developing efficient lattice inclusion host[3] and other useful materials.[4] Single-crystal X-ray diffraction studies on a large number of TAP- and TAMP-based clathrates revealed that the organization of the porphyrin building blocks is strongly conserved.[5] In the absence of specific nonbonded interactions, the tetraphenylporphyrins (TPPs) are packed efficiently in 2D via topological complementarity thereby creating voids in the supramolecular organization which are further filled

* To whom correspondence should be addressed. E-mail: parthod123@rediffmail.com, ocpd@iacs.res.in (P.D.), amitava@csmcri.org (A.D.). Fax: +91-33-2473 2805 (P.D.).

† Central Salt & Marine Chemicals Research Institute (CSIR).

‡ Indian Association for the Cultivation of Science.

(1) *Comprehensive Supramolecular Chemistry*; MacNicol, D. D., Toda, F., Bishop, R., Eds.; Pergamon: Oxford, U.K., 1996; Vol. 6.

(2) Byrn, M. P.; Curtis, C. J.; Hsiou, Y.; Khan, S. I.; Sawin, P. A.; Terzis, A.; Strouse, C. E. In *Comprehensive Supramolecular Chemistry*; MacNicol, D. D., Toda, F., Bishop, R., Eds.; Pergamon: Oxford, U.K., 1996; Vol. 6, p 715.

(3) (a) Harada, R.; Matsuda, Y.; Kawa, H.; Kojima, T. *Angew. Chem., Int. Ed.* **2004**, *43*, 1825. (b) Sharma, C. V. K.; Broker, G. A.; Huddleston, J. G.; Baldwin, J. W.; Metzger, R. M.; Rogers, R. D. *J. Am. Chem. Soc.* **1999**, *121*, 1137. (c) Kosal, M. E.; Suslick, K. S. *J. Solid State Chem.* **2000**, *152*, 87. (d) Abrahams, B. F.; Hoskins, B. F.; Michail, D. M.; Robson, R. *Nature* **1994**, *369*, 727. (e) Goldberg, I. *Chem.*—Eur. J. **2000**, *6*, 3863. (d) Goldberg, I. *Chem. Commun.* **2005**, 1243 and references cited therein. (e) Wojaczyński, J.; Latos-Gra×c0yński, L. *Coord. Chem. Rev.* **2000**, *204*, 113.

10.1021/ic0702163 CCC: $37.00
Published on Web 08/07/2007

by the guest molecules. The porphyrin core can be judicially modified by introducing suitable supramolecular synthons[6] at strategic positions to achieve desired control and robustness in the structure.[7] Another strategy to gain control over the resultant supramolecular structure is to modify the TAMP core via axial coordination to the metal center with a suitable ligand. In this strategy, AMTAMPs (monomer, dimer, oligomers, and polymers) are synthesized and used as novel lattice inclusion hosts. We[8] along with others[9] have shown that by coordinating the metal center of the porphyrin core with pyridyl based ligands, novel AMTAMPs can be created that act as efficient lattice inclusion hosts. The packing of the TPP/TAMP hosts is generally governed by intermolecular porphyrin−porphyrin interactions characterized by primarily C−H···π interactions; parallel chains of porphyrin units are arranged in layers and channels are located between the phenyl arms of the porphyrins (Scheme 1). Similar supramolecular self-assembly is also observed in many such inclusion materials derived from AMTAMPs; while penta- and hexacoordinated TAMP monomeric species are packed in a manner wherein the axial ligands occupy the channel space of the porphyrin arrays along with the guest molecules (if any),[5] the dimer[8,9a−c] and trimer[8] analogues generated by anchoring two and three TAMP units, respectively, also pack in the similar fashion (Scheme 2).

However, the AMTAMPs that have been reported thus far are based on axial modification using pyridyl-based bidentate ligands with linear ligating topology and an innocent backbone. In this context, we are interested in maneuvering the resultant supramolecular organization of AMTAMPs by exploring the study with pyridyl-based bidentate ligands with various angular ligating topologies and a hydrogen bond functionalized (noninnocent) backbone; angular ligating topology of the bidentate ligand is expected to generate a bent multicomponent AMTAMP building block to induce different packing mode, and the hydrogen-bonding backbones would either recognize each other via complementary hydrogen bonding in suitable cases or stabilize the hydrogen bonding capable guest molecules or counteranions, if any, in the resultant lattice.

Scheme 1

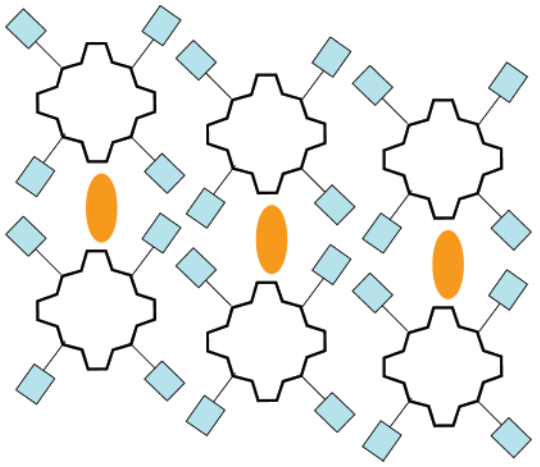

Scheme 2

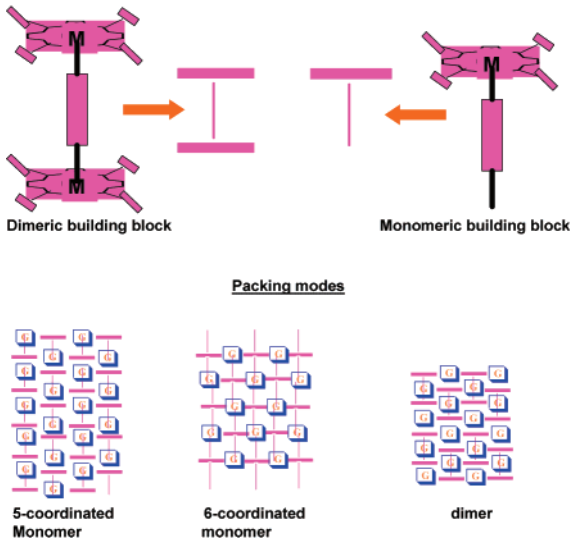

(4) (a) Tao, S.; Li, G.; Zhub, H. *J. Mater. Chem.* **2006**, *16*, 4521. (b) Ogawa, K.; Zhang, T.; Yoshihara, K.; Yoshiaki, K. *J. Am. Chem. Soc.* **2002**, *124*, 22. (c) Lin, V. S.-Y.; DiMagno, S. G.; Therien, M. J. *Science* **1994**, *264*, 1105. (d) Linke, W.; Chambron, J.-C.; Heitz, V.; Sauvage, J.-P. *J. Am. Chem. Soc.* **1997**, *119*, 11329. (e) Wynn, C. M.; Girtu, M. A.; Sugiura, K.-I.; Brandon, E. J.; Manson, J. L.; Miller, J. S.; Epstein, A. J. *Synth. Met.* **1997**, *85*, 1695. (f) Fox, M. A. *Acc. Chem. Res.* **1992**, *25*, 569. (g) Meunier, B. In *Metalloporphyrins Catalysed Oxidations*; Monanari, F., Casella, L., Eds.; Kluwer Academic: Boston, MA, 1994; p 1. (h) Suslick, K. S. Van Deusen-Jefries, S. In *Comprehensive Supramolecular Chemistry: Bioinorganic Systems*; Suslick, K. S., Ed.; Elsevier Science: Oxford, U.K., 1996; Vol. 5, p 733. (i) Harvey, P. D. In *The Porphyrin Handbook*; Kadish, K. M., Smith, K. M., Guilard, R., Eds.; Academic: San Diego, CA, 2003; Vol. 18, Chapter 113.

(5) (a) Byrn, M. P.; Curtis, C. J.; Khan, S. I.; Sawin, P. A.; Tsurumi, R.; Strouse, C. E. *J. Am. Chem. Soc.* **1990**, *112*, 1865. (b) Byrn, M. P.; Curtis, C. J.; Goldberg, I.; Hsiou.; Khan, S. I.; Sawin, P. A.; Tendick, S. K.; Strouse, C. E. *J. Am. Chem. Soc.* **1991**, *113*, 6549. (c) Byrn, M. P.; Curtis, C. J.; Hsiou, Y.; Khan, S. I.; Sawin, P. A.; Tendick, S. K.; Terzis, A.; Strouse, C. E. *J. Am. Chem. Soc.* **1993**, *115*, 9480.

(6) Desiraju, G. R. *Angew. Chem., Int. Ed.* **1995**, *34*, 2311.

(7) (a) Carlucci, L.; Ciani, G.; Proserpio, D. M.; Porta, F. *Angew. Chem., Int. Ed.* **2003**, *42*, 317. (b) Pan, L.; Huang, X.; Phan, H.-L. N.; Emge, T. J.; Li, J.; Wang, X. *Inorg. Chem.* **2004**, *43*, 6878. (c) Hagrman, D.; Hagrman, P. J.; Zubieta, J. *Angew. Chem., Int. Ed.* **1999**, *38*, 3165. (d) Kumar, R. K.; Goldberg, I. *Angew. Chem., Int. Ed.* **1998**, *37*, 3027. (e) Deiters, E.; Bulach, V.; Hosseini, M. W. *Chem. Commun.* **2005**, 3906. (f) Ohmura, T.; Usuki, A.; Fukumori, K.; Ohta, T.; Ito, M.; Tatsumi, K. *Inorg. Chem.* **2006**, *45*, 7988. (g) Kosal, M. E.; Chou, J.-H.; Wilson, S. R.; Suslick, K. S. *Nat. Mater.* **2002**, *1*, 118. (h) Diskin-Posner, Y.; Dahal, S.; Goldberg, I. *Chem. Commun.* **2000**, 585. (i) Goldberg, I.; Muniappan, S.; George, S.; Lipstman, S. *CrystEngComm* **2006**, *8*, 784. (j) Ring, D. J.; Aragoni, M. C.; Champness, N. R.; Wilson, C. *CrystEngComm* **2005**, *7*, 621. (k) Kempea, R.; *Z. Anorg. Allg. Chem.* **2005**, *631*, 1038. (l) Bharyappa, P.; Wilson, S. R.; Suslick, K. S. *J. Am. Chem. Soc.* **1997**, *119*, 8492.

(8) Shukla, A. D.; Dave, P. C.; Suresh, E.; Das, A.; Dastidar, P. *J. Chem. Soc., Dalton Trans.* **2000**, 4459.

(9) (a) Diskin-Posner, Y.; Patra, G. K.; Goldberg, I. *J. Chem. Soc., Dalton Trans.* **2001**, 2775. (b) Kumar, R. K.; Diskin-Posner, Y.; Goldberg, I. *J. Inclusion Phenom. Macrocyclic Chem.* **2000**, *37*, 219. (c) Kumar, R. K.; Balasubramanian, S.; Goldberg, I. *Chem. Commun.* **1998**, 1435. (d) Konarev, D. V.; Litvinov, A. L.; Neretin, I. S.; Drichko, N. V.; Slovokhotov, Y. L.; Lyubovskaya, R. N.; Howard, J. A. K.; Yufit, D. S. *Cryst. Growth Des.* **2004**, *4*, 643. (e) Alessio, E.; Geremia, S.; Mestroni, S.; Iengo, E.; Srnova, I.; Slouf, M. *Inorg. Chem.* **1999**, *38*, 869. (f) Tat, F. T.; Zhu, Z.; MacMahon, S.; Song, F.; Rheingold, A. L.; Echegoyen, L.; Schuster, D. I.; Wilson, S. R. *J. Org. Chem.* **2004**, *69*, 4602. (g) Choi, M. T. M.; Choi, C.-F.; Ng, D. K. P *Tetrahedron* **2004**, *60*, 6889. (h) D'Souza, F.; Rath, N. P.; Deviprasad, G. R.; Zandler, M. E. *Chem. Commun.* **2001**, 267. (i) Wyllie, G. R. A.; Schulz, C. E.; Scheidt, W. R. *Inorg. Chem.* **2003**, *42*, 5722. (j) Burrell, A. K.; Jones, B. M.; Hall, S. B.; Officer, D. L.; Reid, D. C. W.; Wild, K. Y. *J. Inclusion Phenom. Macrocyclic Chem.* **1999**, *35*, 185. (k) Ikeda, T.; Asakawa, M.; Goto, M.; Nagawa, Y.; Shimizu, T. *Eur. J. Org. Chem.* **2003**, 3744.

ZnTPP is found to be a much better general purpose host for the design of inclusion materials. Double occupation of the $d_{x^2-y^2}$ orbital of the Zn^{2+} complex tends to increase the metal−nitrogen bond distances and destabilizes the ruffled conformation of the porphyrin plane observed in TPP complexes with other first row transition metals. Thus, the more planar ZnTPP has higher symmetry and provides fewer orientational degrees of freedom, thereby making it a potential building block. Moreover, Zn^{2+} displays high affinity for pentacoordinated environment thereby making it a suitable candidate for dimeric AMTAMPs and in some rare occasion trimeric[8] AMTAMPs wherein both penta- and hexacoordinated metal centers are present, whereas Mn^{3+} has a strong tendency to form hexacoordinated environment thereby making it a good candidate for polymeric AMTAMPs although only few TPP-based coordination polymers are thus far reported.[7d,9a,c] We have been studying the role of various bis(pyridyl) ligands having different hydrogen bonding capable backbones and ligating topologies on the resulting supramolecular structures of various metal−organic frameworks (MOFs).[10] In this context, we considered it worthwhile to modify TAMP by axially coordinating the porphyrin core using some of these bis(pyridyl) ligands.

Thus, we have studied nine inclusion crystals derived from AMTAMPs generated by axially modifying ZnTPP/MnTPP•Cl by three pyridyl-based ligands, namely *N*,*N*′-bis(4-pyridyl)urea (**4BPU**),[11] *N*,*N*′-bis(3-pyridyl)urea (**3BPU**),[11] and *N*-(4-pyridyl)isonicotinamide (**4PIN**).[12] Supramolecular structures of these AMTAMPs in the resultant inclusion crystals and their thermal behavior are reported.

Results and Discussion

Synthesis. Our previous encounter with AMTAMPs synthesis suggests that stoichiometric amount of the reactants namely TAMP and a bidentate ligand does not yield dimeric building block;[8] twice an excess of the bidentate ligand is a requirement. Thus, in this study, the reactants are taken in TAMP−bidentate ligand (1:2) ratio and crystallized from suitable solvent systems with the hope of obtaining dimeric AMTAMPs. A total of 11 inclusion crystals namely **10**−**20** were isolated (Scheme 3). Crystals suitable for single-crystal X-ray diffraction are chosen and structurally characterized. However, crystal structures of **10** and **17** could not be fully determined. Crystal data for **11**−**16** and **18**−**20** are listed in Table 1. Thermogravimetric analyses of all the inclusion crystals except **12** and **15** are listed in Table 2. Crystals of **12** and **15** are found to be too unstable to perform TGA experiments.

Scheme 3 depicts the chemical structure of the reactants, molecular structures of the AMTAMPs as observed in the corresponding X-ray structures of the inclusion materials, the composition of the inclusion materials thus derived, and the solvent combination used for crystallization (given in parentheses) reported in this study. As expected, except **2** and **5**, all the building blocks are dimers in ZnTPP-based compounds; relatively high thermodynamic stability of the binuclear complex[13] along with strong affinity of pentacoordination of Zn^{2+} ion probably induces the formation of a dimeric building block. However, pentacoordinated monomeric building blocks derived from ZnTAP and bidentate ligands are rare and **2** and **5** are probably the first such examples in the literature.[14] It is interesting to note that when the crystals of **12** comprised of monomeric building block **2** are dissolved in DMF and recrystallized, inclusion crystals of **11** containing the dimeric building block **1** are formed indicating the preferences for forming dimeric building block in ZnTPP-based materials. On the other hand, Mn^{3+} in MnTPP•Cl prefers a hexacoordinated geometry of the metal center and, thus, formation of either coordination polymer or discrete hexcoordinated monomer is expected. Out of three inclusion materials based on MnTPP•Cl reported herein (**18**−**20**), inclusion material **18** is based on coordination of a polymeric building block, namely, **7**; the other two, **19** and **20**, are based on hexacoordinated monomeric building block **8**.

Molecular Structure of the AMTAMPs As Observed for the Corresponding Inclusion Crystals. The porphyrin cores are found to be reasonably planar in all the building blocks. While pentacoordinated Zn^{2+} metal ions of the AMTAMPs **1**−**5** are slightly away from the porphyrin core by 0.211−0.416 Å, hexacoordinated Mn^{3+} ions are located on the mean porphyrin plane in **7** and **8**. Zn−N_{axial} and Mn−N_{axial} bond distances are within the usually observed ranges of 2.105(6)−2.217(6) and 2.216(6)−2.224(5) Å, respectively.

Dimeric AMTAMPs. Among the axial ligands used in this study, the ligating topologies of **4PIN** and **4BPU** are conformation independent and almost linear although not as linear as their counter analogue, namely, 4,4′-bipyridine, whereas **3BPU** which is a positional isomer of **4BPU** that can have different ligating topologies depending on its conformation. While *syn*−*syn* conformation would lead to an angular ligating topology, *anti*−*anti* conformation will result into a linear ligating topology in **3BPU**. Thus, the AMTAMPs derived from **4PIN** and **4BPU** are expected to form slightly bent dumbbell-shaped dimeric complexes whereas the shape of the building block generated by *syn*−*syn* **3BPU** would be a severely bent dumbbell and that generated by *anti*−*anti* **3BPU** would be a linear dumbbell. When analyzed, it is observed that the dimeric building block **4** in **15** generated by **4PIN** is a perfectly linear dumbbell displaying 0.0° angle between the terminal porphyrin cores. Meanwhile **3**, the building block observed in the inclusion crystals **13** and **14**, displays a severely bent dumbbell shape

(10) (a) Krishna Kumar, D.; Jose, D. A.; Das, A.; Dastidar, P. *Inorg. Chem.* **2005**, *44*, 6933. (b) Krishna Kumar, D.; Das, A.; Dastidar, P. *New J. Chem.* **2006**, *30*, 1267. (c) Krishna Kumar, D.; Das, A.; Dastidar, P. *Cryst. Growth Des.* **2006**, *6*, 1903. (d) Krishna Kumar, D.; Das, A.; Dastidar, P. *J. Mol. Struct.* **2006**, *796*, 139. (e) Krishna Kumar, D.; Das, A.; Dastidar, P. *CrystEngComm.* **2006**, 805.

(11) Krishna Kumar, D.; Jose, D. A.; Das, A.; Dastidar, P. *Chem. Commun.* **2005**, 4059.

(12) Krishna Kumar, D.; Jose, D. A.; Dastidar, P.; Das, A. *Langmuir* **2004**, *20*, 10413.

(13) Das, A.; Maher, J. P.; McCleverty, J. A.; Badiola, J. A. N.; Ward, M. D. *J. Chem. Soc., Dalton Trans.* **1993**, 681.

(14) CCDC search (CSD 5.27, Nov 2005 release) of a fragment containing metalated TPP (any transition metal) coordinated by pyridyl fragment did not show any report of pentacoordinated monomer wherein the axial ligand is a pyridyl-based bidentate ligand.

Scheme 3

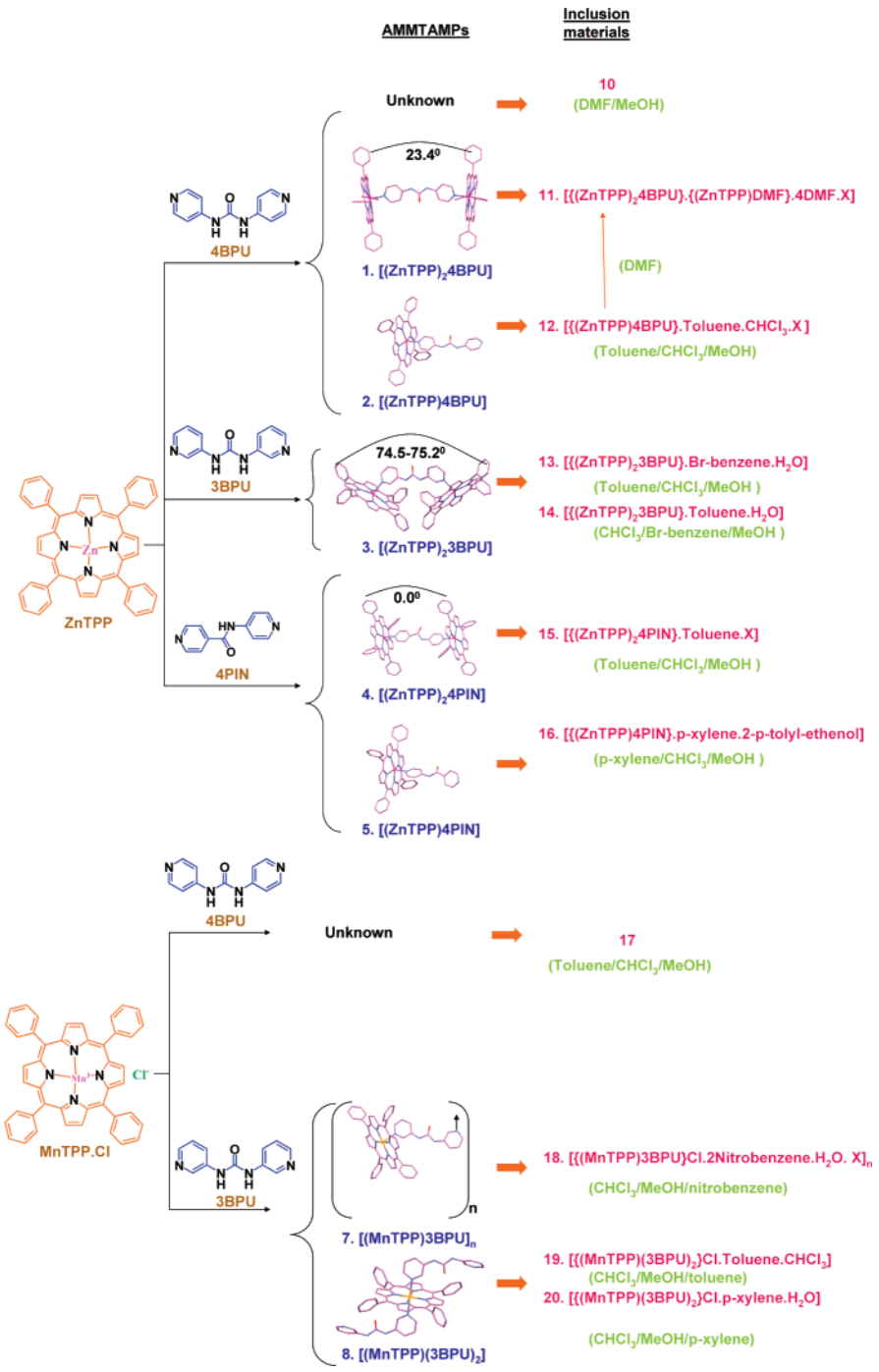

with the corresponding porphyrin−porphyrin angles of 74.5 and 75.2°, respectively, which is expected because of the *syn*−*syn* conformation of **3BPU**. On the other hand, the dimeric building block **1** in **11** displays a porphyrin−porphyrin angle of 23.4°, which appears to be as a result of the slightly angular ligating topology of **4BPU**.

Polymeric AMTAMPs. 3BPU results in a polymeric building block owing to the fact that Mn^{3+} prefers a hexacoordinated environment. The polymeric AMTAMP **7**, found in inclusion crystal **18**, displays a linear propagation due to the linear ligating topology of the *anti*−*anti* conformation of **3BPU**. Thus, the porphyrin−porphyrin angle in this polymeric AMTAMP is found to be 36.5°.

Monomeric Pentacoordinated AMTAMPs. As discussed earlier, generating pentacoordinated AMTAMPs using ZnTPP and/or MnTPP and a bidentate ligand is extremely difficult and there is no guarantee of its successful synthesis. However, in this study, two such pentacoordinated monomers, namely, **2** and **5** are observed in the inclusion crystals **12** and **16**, respectively. In both the cases, the molecular topology of the building block can be best described as a "board pin" shaped complex emphasizing the fact that the bidentate pyridyl ligands approached the metal center in a near perfect axial direction which is characterized by ~90.0° angle involving pyridyl N, metal center, and pyrrole N of the porphyrin core.

Table 1. Crystal Data

Crystal data	**11**	**12**	**13**	**14**	**15**
Empirical formula	$C_{158}H_{122}N_{21}O_6Zn_3$	$C_{62.33}H_{46.33}ClN_8OZn$	$C_{61.50}H_{44}Br_2N_6OZn$	$C_{63.5}H_{50}N_6OZn$	$C_{56.5}H_{40}N_{5.5}O_{0.5}Zn$
Formula weight	2606.88	1024.23	1108.22	978.47	869.31
Crystal size (mm)	0.40 × 0.18 × 0.06	0.26 × 0.22 × 0.12	0.26 × 0.21 × 0.06	0.30 × 0.12 × 0.05	0.30 × 0.24 × 0.08
Crystal system	Triclinic	Trigonal	Monoclinic	Monoclinic	Triclinic
Space group	P-1	R-3	*C*2	*C*2	P-1
a (Å)	13.3651(8)	39.6465(13)	18.5409(17)	18.5279(11)	11.170(3)
b (Å)	17.5105(10)		11.9085(11)	11.8843(7)	11.284(3)
c (Å)	28.9961(17)	17.0551(12)	23.836(2)	23.8153(15)	22.556(6)
α (^{0})	92.6800(10)				80.641(4)
β (^{0})	91.1970(10)		110.051(2)	109.5620(10)	86.847(6)
γ (^{0})	93.4930(10)	120.00			73.517(5)
Volume (Å^3)	6764.0(7)	23216(2)	4943.9(8)	4941.2(5)	2689.8(12)
Z	2	18	4	4	2
$D_{calc.}$(g/cm^3)	1.280	1.319	1.489	1.315	1.073
F(000)	2710	9564	2252	2044	903
μ MoKα (mm^{-1})	0.594	0.579	2.164	0.548	0.495
Temperature (K)	298(2)	100(2)	100(2)	100(2)	100(2)
Range of h, k, l	−17/17, −23/23, −38/38	−47/45, −41/47, −18/20	−22/22, −14/14, −28/28	−19/24, −15/14, −30/26	−14/12, −14/9, −28/29
θ min/max	1.17/28.29	1.68/25.00	1.82/25.00	2.07/28.26	1.83/28.37
Reflections collected/ unique/observed	78134/31309/22287	38435/9092/7356	23414/4580/4125	14456/5946/5452	15586/11589/5117
Data/restraints/ parameters	31309/0/1665	9092/0/650	4580/1/650	5946/1/652	11589/1/524
Goodness of fit on F^2	1.043	0.965	1.012	1.017	0.872
Final R indices [I > 2σ(I)]	R_1 = 0.0655	R_1 = 0.0692	R_1 = 0.0378	R_1 = 0.0351	R_1 = 0.0819
	wR_2 = 0.1604	wR_2 = 0.2063	wR_2 = 0.0893	wR_2 = 0.0798	wR_2 = 0.2005
R indices (all data)	R_1 = 0.0939	R_1 = 0.0787	R_1 = 0.0440	R_1 = 0.0395	R_1 = 0.1723
	wR_2 = 0.1730	wR_2 = 0.2149	wR_2 = 0.0924	wR_2 = 0.0817	wR_2 = 0.2361

Crystal data	**16**	**18**	**19**	**20**
Empirical formula	$C_{72}H_{57}N_7O_2Zn$	$C_{67}H_{48}ClMnN_{10}O_6$	$C_{74}H_{53}Cl_4MnN_{12}O_2$	$C_{78}H_{63}ClMnN_{12}O_3$
Formula weight	1117.62	1179.54	1339.02	1306.79
Crystal size (mm)	0.40 × 0.18 × 0.05	0.20 × 0.13 × 0.02	0.40 × 0.28 × 0.05	0.34 × 0.18 × 0.04
Crystal system	Monoclinic	Triclinic	Triclinic	Triclinic
Space group	$P2_1$/c	P-1	P-1	P-1
a (Å)	11.682(2)	12.9200(12)	12.9146(17)	12.8727(11)
b (Å)	23.694(5)	13.9061(12)	15.739(2)	13.0713(11)
c (Å)	22.016(4)	16.0531(14)	17.626(2)	20.0292(16)
α (^{0})		93.852(2)	92.632(2)	82.5140(10)
β (^{0})	104.749(3)	94.519(2)	110.355(2)	84.0510(10)
γ (^{0})		96.530(2)	105.793(2)	78.2670(10)
Volume (Å^3)	5894(2)	2848.1(4)	3192.7(7)	3261.3(5)
Z	4	2	2	2
$D_{calc.}$(g/cm^3)	1.260	1.375	1.393	1.331
F(000)	2336	1220	1380	1362
μ MoKα (mm^{-1})	0.470	0.343	0.433	0.305
Temperature (K)	150(2)	100(2)	150(2)	100(2)
Range of h, k, l	−15/15, −23/31, −28/27	−15/15, −16/16,-19/19	−15/17, −18/20, −23/20	−16/16, −16/17, −26/26
θ min/max	1.29/28.41	1.28/25.00	1.25/28.26	1.60/28.34
Reflections collected/ unique/observed	34323/13576/6859	20614/9972/6407	17942/13606/8192	36619/14928/10100
Data/restraints/parameters	13576/0/731	9972/0/699	13606/0/836	14928/0/878
Goodness of fit on F^2	0.939	1.042	1.022	1.042
Final R indices [I > 2σ(I)]	R_1 = 0.0579	R_1 = 0.0964	R_1 = 0.0686	R_1 = 0.0575
	wR_2 = 0.1506	wR_2 = 0.2091	wR_2 = 0.1637	wR_2 = 0.1462
R indices (all data)	R_1 = 0.1308	R_1 = 0.1468	R_1 = 0.1273	R_1 = 0.0955
	wR_2 = 0.1910	wR_2 = 0.2323	wR_2 = 0.1887	wR_2 = 0.1659

Monomeric Hexacoordinated AMTAMPs. Hexacoordinated monomeric AMTAMPs are observed only in the inclusion materials of MnTPP•Cl since Mn^{3+} prefers a hexacoordinated environment. Hexacoordinated monomeric building block **8** is observed in the corresponding inclusion crystals **19** and **20**. The axial ligand **3BPU** in both the crystallographically independent building blocks located in the asymmetric unit of **19** displays a nonplanar *syn*−*syn* conformation with pyridyl−pyridyl angles of 33.6 and 58.2°, respectively. An almost identical molecular topology of the building block is observed in **20** except that here the pyridyl−pyridyl angles of **3BPU** observed in the two crystallographically independent building blocks are 31.3 and 51.8°, respectively.

Supramolecular Architectures of the AMTAMPs Inclusion Host in the Crystal Structures of the Corresponding Inclusion Materials. Dimeric AMTAMPs. Dimeric building blocks are observed in the inclusion materials derived from ZnTPP. All the three axial ligands, namely, **4BPU**, **3BPU**, and **4PIN** result in dimeric building blocks

Table 2. Thermogravimetric Data

wt loss % obsd	wt loss % calcd	peak temp/°C	loss of
		11	
14.8	14.1	146.0	5 DMF, 1 H_2O
10.8	10.5	212.8	1 DMF, 1 **4BPU**
		13	
30.5	29.1	122.9	4 bromobenzene, 1 H_2O
10.8	9.6	247.4	1 **3BPU**
		14	
10.9	10.3	131.6	2 toluene, 1 H_2O
20.8	20.3	250.1	2 toluene, 1 **3BPU**
		16	
21.5	21.4	151.0	1 *p*-xylene, 1 2-*p*-tolylethenol
18.6	17.8	264.6, 303.4	1 **4PIN**
		18	
20.8	23.5	110.1	2 nitrobenzene, 2 H_2O
18.6	17.8	281.5	1 **3BPU**
		19	
15.7	15.7	144.7	1 toluene, 1 $CHCl_3$
31.9	31.9	229.6, 287.0	2 **3BPU**
		20	
12.9	12.1	67.5, 136.6	1.5 *p*-xylene
34.8	34.1	216.2, 266.5	2 **3BPU**, 1 H_2O

in the corresponding inclusion materials, namely, **11**, **13** and **14**, and **15**, respectively.

[{(ZnTPP)$_2$4BPU}·{(ZnTPP)DMF}·4DMF·X] (11). One dimeric building block **1**, one pentacoordinated ZnTPP wherein the axial site is occupied by the O atom of DMF, three DMF guests, one disordered DMF, and unaccountable electron densities presumably from disordered DMF are located in the asymmetric unit of **11**. Since the smeared electron densities could not be modeled properly, the overall contribution of the unaccounted electron densities to the diffraction pattern is subtracted from the observed data using a "bypass" technique, namely, SQUEEZE;[15] subsequent refinement with these relatively "noisefree" data enabled a reasonable refinement of the structure.

The slightly bent dumbbell shaped dimers are packed in a linear fashion via porphyrin−porphyrin interactions resulting into the formation of a microporous ladder architecture. The ladders are then further packed in an offset fashion thereby blocking the pores of the ladders. However, a multipore architecture is formed along the ladder axis and pores are located between the offsetly packed ladder assemblies. Smaller voids are located between the axial ligands of the building blocks whereas the bigger one is located among the porphyrin arms. While one of the three ordered DMF molecules forms a bifurcated hydrogen bonding with the urea funcationality [N···O = 2.786(3)−3.122(3) Å; ∠N−H···O = 169.2−146.2°], the other two are located in the bigger void. The disordered DMF is located near the smaller void. The bigger void is also occupied by the pentacoordinated ZnTPP−DMF complex as guest. The disordered DMFs for which no suitable model could be refined are located in the smaller voids (Figure 1). Squeezed electrons (97 e/unit cell) probably indicate the presence of two DMF's and two water molecules. Thermal analyses also support these data (Table 2).

(15) Van der Sluis, P.; Spek, A. L. *Acta Crystallogr.* **1990**, *A46*, 194.

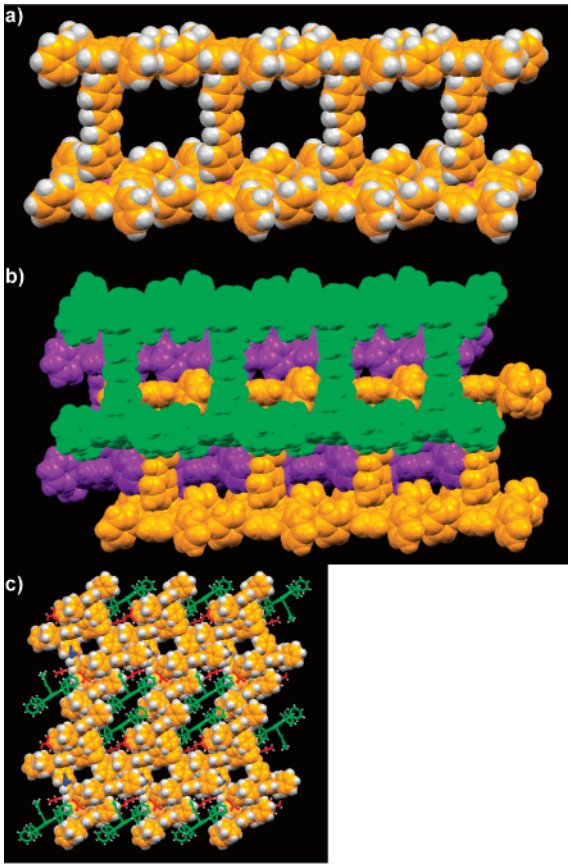

Figure 1. Crystal structure illustration of **11**: (a) 1D ladder type array of the dimeric building block **1** showing open voids; (b) offset pack of the ladder blocking the voids; (c) overall packing viewed down the ladder propagation axis displaying multipore architecture wherein the guest molecules (green, ZnTPP−DMF; red, ordered DMF; blue, disordered DMF) are located.

[{(ZnTPP)$_2$3BPU}·Br-benzene·H$_2$O] (13). The asymmetric unit of **13** contains half of the dimer **3** (the urea C═O of which is sitting on a 2-fold axis), a half-water molecule [also sitting on the 2-fold and hydrogen bonded to urea functionality via N−H···O interactions (N···O = 2.930(8) Å; ∠N−H···O = 158.9°)], and two bromobenzenes located on general positions. The dimers are found to be propagating along *c*-axis in a linear fashion apparently directed by porphyrin−porphyrin interactions. The 1D arrays of the dimer are then packed in a parallel fashion resulting in a 2D porous architecture. The guest molecules, namely, bromobenzene are located within the pores. Such 2D layers are further packed in an offset fashion (Figure 2). TGA data match well with the X-ray results (Table 2).

The dimer **3** seen in the inclusion material [{(ZnTPP)$_2$**3BPU**}·toluene·H$_2$O] **(14)** also adopts a near identical supramolecular assembly as observed in **13**. In fact, both these inclusion materials **13** and **14** display an identical space group (*C*2) and very similar cell dimensions. In this inclusion crystal of **14**, the guest molecules are toluene and water. TGA analyses (Table 2) also support the crystallographic finding.

[{(ZnTPP)$_2$4PIN}·toluene·X] (15). The dimeric building block **4** is found to be disordered in the crystal structure of **15** around a center of symmetry which may be arising due to the statistical centrosymmetric arrangement of the axial

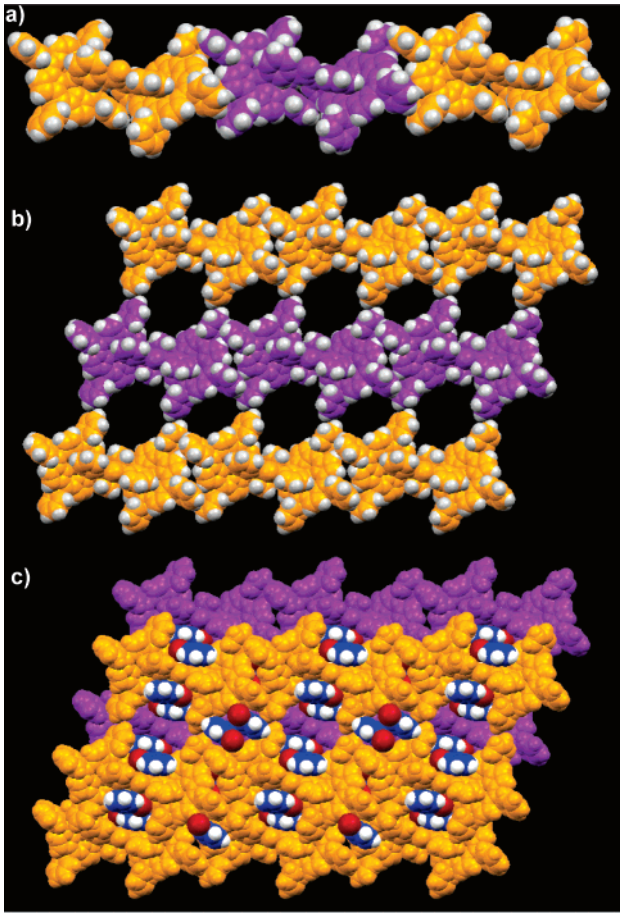

Figure 2. Crystal structure illustration of **13**: (a) 1D array of the bent dimer **3**; (b) 2D sheet structure of the 1D array (shown in alternating orange and purple color) displaying voids; (c) offset packing of the 2D sheets (shown in purple and orange) and guest occlusion (blue−white−magenta, bromobenzene). The water guest is embedded within the dimer via hydrogen bond with urea functionality and not seen here.

ligand, namely, **4PIN**. Thus, the asymmetric unit is comprised of half of the disordered dimer, one toluene molecule, and a disordered toluene molecule. In the final refinement, however, the disordered toluene molecule is squeezed[15] out (see above) because it could not be refined; only the disordered dimer and one toluene guest are refined. The dimers are packed via porphyrin−porphyrin interactions approximately along the diagonal of the *a*−*b* plane thereby creating a 1D ladder type microporous architecture. The 1D arrays are further packed in an offset manner so that various voids are created in the hierarchical assembly. The toluene guest is found to be arrested in the cage type of voids among the porphyrin moieties. Open channels are also seen between the offsetly packed ladders; the channels are most probably accommodated by the disordered toluene (Figure 3). However, SQUEEZE[15] calculations (see above) indicated the presence of 72 e/unit cell, which is 28 e less than that expected for two disordered toluene molecules in the unit cell. This is not surprising as the crystal mounted for X-ray diffraction was deteriorating fast and, therefore, the residual electron densities for the disordered toluene was less than expected. TGA analyses could not be performed for these crystals because of their fast deterioration.

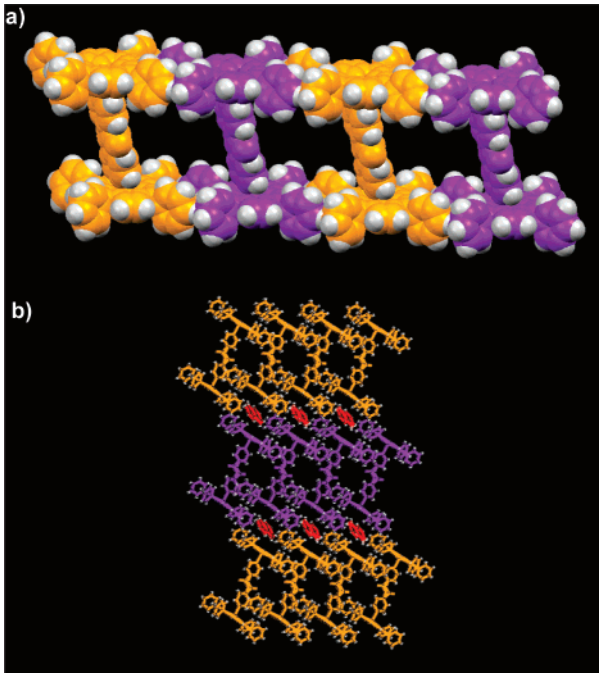

Figure 3. Crystal structure illustration of **15**: (a) 1D ladder type of array of the dimeric building block **4** displaying pores; (b) overall packing viewed down the ladder propagation axis. The ordered toluene guests (red) are located in the cages generated by the porphyrin moieties; disordered guest molecule (not shown) are located in the bigger channels generated near the axial ligand moieties.

Polymeric AMTAMPs. Polymeric building blocks are observed in the inclusion materials derived from MnTPP•Cl. **3BPU** results in a polymeric AMTAMP in the corresponding inclusion crystals **18**.

[{(MnTPP)3BPU}Cl·2-nitrobenezene·H_2O·X]$_n$ (18). One axial ligand **3BPU**, two half-MnTPP moieties for which the Mn centers lie on center of symmetries, a Cl^- ion, two nitrobenzenes, and one water molecule are located in the asymmetric unit of **18**. At the end of the final cycles of refinement, some disordered electron densities were also located. SQUEEZE[15] calculation (see above) indicated the presence of 11 e/unit cell which amounts to one disordered water molecule. TGA results are also commensurate with these findings (Table 2). In the crystal structure, the axial ligand which shows an *anti*−*anti* conformation coordinates to the adjacent MnTPP moieties resulting in the formation of a linear coordination polymer which passes through the center of the *a*−*c* plane and center of the *b*-axis. The 1D linear polymeric chains are further packed in a parallel fashion resulting in the formation of a 2D layer structure. The porphyrin moieties are approximately perpendicular to the layer. Thus, when these layers pack in the third dimension, it results in the formation of cage architecture within which the guest molecules (nitrobenzene and water) are accommodated (Figure 4).

Pentacoordinated Monomeric AMTAMPs. Pentacoordinated monomeric building blocks are observed only in two cases, namely, in the crystals of **12** and **16**.

[{(ZnTPP)4BPU}·toluene·$CHCl_3$·X] (12). The asymmetric unit contains one monomer **2**, one toluene, one $CHCl_3$ sitting on a 3-fold axis, and several electron density peaks

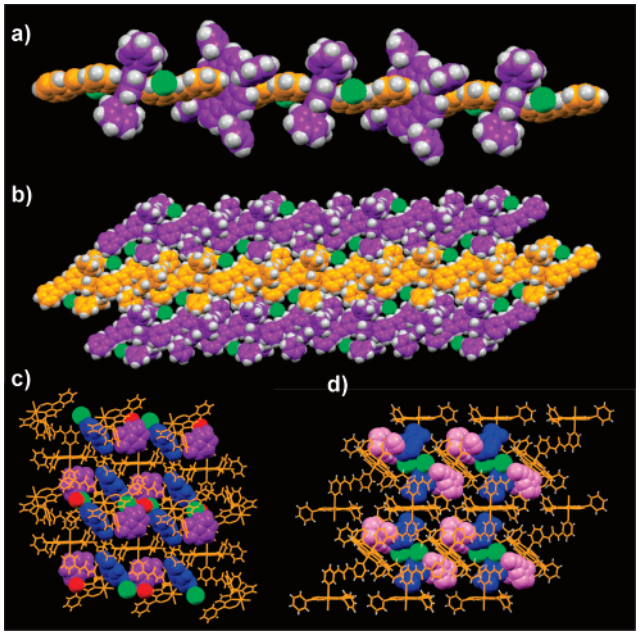

Figure 4. Crystal structure illustration of **18**: (a) 1D linear coordination polymeric building block **7**; (b) parallel packing of the polymeric chains resulting in 2D layer structure displaying Cl^- ions association with the urea functionality; (c) packing of the 2D layers creating cage architecture within which guest molecules (pink and blue = nitrobenzene; red = water) are located; (d) another view of the overall packing.

which appear to be a disordered toluene. In the final refinement, the unaccounted electron densities are squeezed[15] out (see above) and only the host moiety and ordered guest molecules, namely, toluene and $CHCl_3$ are refined.

In the crystal structure, each monomer is involved in hydrogen bonding with two neighboring monomers via N−H···N hydrogen bonding involving N−H of urea and N of the pyridyl moiety [N···N = 2.901(5) Å; ∠N−H···N = 163.7°]. Such interactions lead to the formation of a 1D hydrogen-bonded chain displaying 3-fold symmetry. The 1D chains are further packed in a parallel fashion resulting in the formation of an architecture containing voids within which the guest molecules are occluded (Figure 5). SQUEEZE[15] calculations (see above) showed the presence of 380 e/unit cell which may be attributed to 8 toluene molecules. TGA analyses did not give satisfactory results presumably due to the escape of the guest molecules at room temperature.

[{(ZnTPP)4PIN}·*p*-xylene·2-*p*-tolylethenol] (16). The asymmetric unit of **16** contains one monomer **5**, one *p*-xylene, and one 2-*p*-tolylethenol. The presence of 2-*p*-tolylethenol in the crystal structure is a surprise inclusion of the alcohol impurity presumably coming from the *p*-xylene used for crystallization. In the crystal structure, the monomeric unit is involved in hydrogen-bonding interactions with the alcohol guest via N−H···O and O−H···N interactions [N···O = 2.949(5) Å; ∠N−H···O = 156.9°; O···N = 2.762(4) Å; ∠O−H···N = 171.0(4)°] around a center of symmetry so that a guest-mediated hydrogen-bonded dimer of the monomer **5** is formed. The hydrogen-bonded dimers are further packed in herringbone fashion entrapping the *p*-xylene guest molecules in the lattice (Figure 6). TGA data match well with the X-ray structure (Table 2).

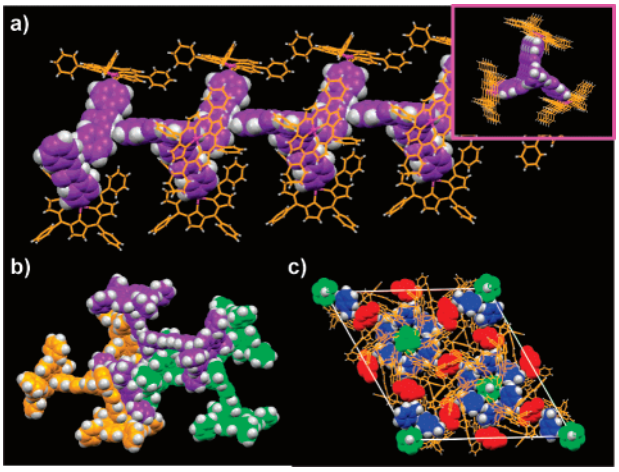

Figure 5. Crystal structure illustration of **12**: (a) hydrogen-bonded 1D array of pentacoordinated dimeric building block **2** (inset: axial view of 1D chain displaying 3-fold symmetry); (b) association of the hydrogen-bonded chains (interacting chains shown in orange, purple, and green); (c) overall packing displaying cage architecture within which the guest molecules (toluene, blue/white; $CHCl_3$, green/white; disordered guest, red) are located.

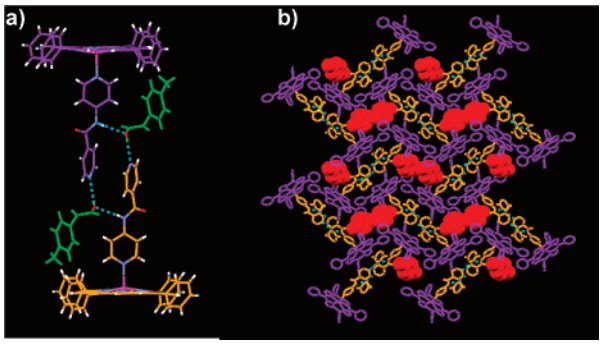

Figure 6. Crystal structure illustration of **16**: (a) hydrogen-bonded guest (2-*p*-tolylethenol, green) mediated dimer of pentacoordinated monomeric building block **5**; (b) herringbone packing of the hydrogen-bonded dimer (purple−orange) displaying entrapment of the guest (*p*-xylene, red).

Hexacoordinated Monomers of AMTAMPs. Hexacoordinated AMTAMPs are observed in MnTPP-derived inclusion crystals **19** and **20**.

[{(MnTPP)(3BPU)$_2$}Cl·toluene·CHCl$_3$] (19). The asymmetric unit of **19** contains two half-moieties of MnTPP, one $CHCl_3$, one toluene (the Me group of which is disordered over two places), and a Cl^- ion. The counterion Cl^- forms a hydrogen bond with both the monomers via N−H···Cl hydrogen bonding, while it is involved in hydrogen-bonding interactions with both the N−H of one monomer [N···Cl = 3.163(3)−3.237(4) Å; ∠N−H···Cl = 150.8−153.9°] and the other monomer interacts with the Cl^- ion via one N−H of the urea moiety [N···Cl = 3.220(4) Å; ∠N−H···Cl =163.6)°]. The metal centers Mn of both the MnTPP moieties sit on a center of symmetry. There are two crystallographically independent monomers in the crystal structure. One of the monomers packs along the *b*−*c* plane generating an architecture containing voids. Further packing analyses reveals that these voids are occupied by the second monomers as well as the guest molecules (Figure 7). TGA data (Table 2) also support these findings.

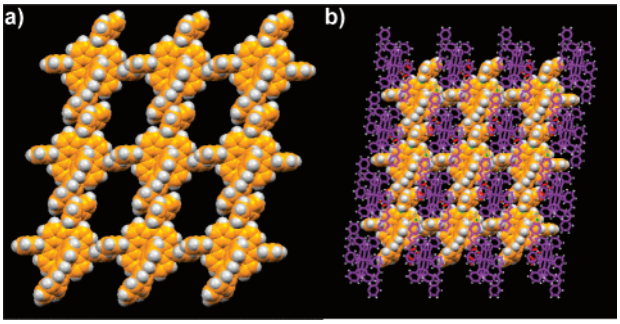

Figure 7. Crystal structure illustration of **19**: (a) void containing 2D array of one of the hexacoordinated monomers in the asymmetric unit; (b) overall packing showing the other crystallographically independent monomer occupying the voids. The guest molecules toluene and $CHCl_3$ (red) also occupy the voids.

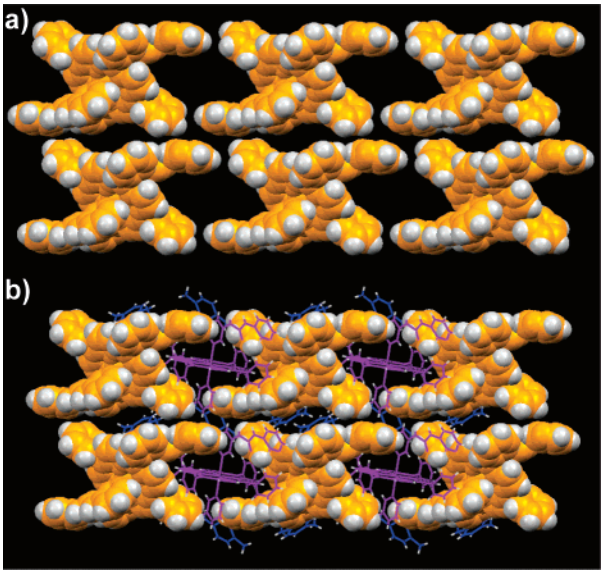

Figure 8. Crystal structure illustration of **20**: (a) 2D array of one of the hexacoordinated monomers displaying two differently sized voids; (b) overall packing showing how the other monomer (purple) and *p*-xylene (blue) occupy the voids.

[{(MnTPP)(3BPU)$_2$}Cl·*p*-xylene·H$_2$O] (20). Structural analyses reveal that inclusion crystal **20** is a supramolecular isomer[16] of **19**. The asymmetric unit is comprised of two independent monomers like in **19**, two *p*-xylenes (one of them residing on a center of symmetry), one water, and a Cl^- ion. Thus, the host building block is identical with that observed in **19**. However, the supramolecular architecture of the host building block in **20** is entirely different from that observed in **19** thereby making it a supramolecular isomer of **19**. In this structure, one of the crystallographically independent dimers packs along the *a*−*c* plane resulting in the formation of a 2D layer structure containing two different types of voids. The larger voids are then occupied by the second monomer, and the smaller one is filled with *p*-xylene (Figure 8). The water molecule is found to be hydrogen bonded with the uncoordinated pyridine moiety of the one of the monomers via O−H···N interactions [O···N = 2.928 Å (H of water could not be located; thus, the angular parameter is not available)]. The counterion Cl^- is involved in hydrogen bonding with both the monomers. While it forms hydrogen bonding with both the urea N−H's of one monomer [N···Cl = 3.212−3.227 Å; ∠N−H···Cl = 159.0(3)−161.0(3)°], it also acts as hydrogen bond acceptor and interacts with one of the urea N−H's of the other monomer [N···Cl = 3.201(3) Å; ∠N−H···Cl = 169(3)°]. TGA data also corroborate well with the X-ray structure (Table 2).

A CSD (CSD 5.27, Nov 2005 release) search conducted with a search fragment containing a metallo-TPP (only transition metal) coordinated with a pyridyl moiety results in 63 hits out of which 7 pentacoordinated monomers, 5 hexacoordinated monomers, 13 dimers, and 3 polymers are observed; there is only one structure (reference code: HALXIB) wherein the axial ligand is 4-methylpyridine conforms to the packing mode depicted for pentacoordinated momomeric species (Scheme 2). The rest of the six structures (reference codes: MOSFOP, MOSFIJ, HUCNAU, DACNIF, MOSFUV, NIOJOM) display different packing modes probably due to strong interactions with the π-surface of the porphyrin moiety, and C_{60}, C_{70}, and porphyrin moieties used in the axial ligand thereby display significant consequences on the packing modes.

The monomeric building block **2** observed in the inclusion crystal **12** does not conform to the packing modes of pentacoordinated monomeric species as depicted in Scheme 2. Due to hydrogen-bonding interactions among the axial ligands **4BPU**, it forms a 1D chain with 3-fold symmetry resulting in the formation of an intriguing packing mode. On the other hand, the monomeric building block **5** observed in the inclusion crystal **16** self-assembles to form a hydrogen-bonded dimer involving the alcohol guest. However, such dimers do not pack in the way depicted in Scheme 2. It rather prefers to pack in a herringbone fashion maximizing the interactions between the axial ligand moieties (in the present case, both axial ligand **4PIN** and the alcohol guest) with the porphyrin moiety of the building block as also observed in some dimeric structures such as BABBIQ. It may be noted that both the structures **12** and **16** display porphyrin−porphyrin interactions characterized by various C−H···π interactions[17] (3.601−3.808 Å) as observed in many TPP-based inclusion crystals.

The dimer in **11** adopts a slightly bent topology and displays a similar, although not identical, packing observed for linear dimers (Scheme 2); the little difference appears to be arising due to its need to accommodate a guest as large as a DMF-coordinated ZnTPP.

Dimer **3** (as observed in both **13** and **14**) displays a severely bent topology. However, it packs in a manner never observed before in a pyridyl-based metallo-TPP dimer. C−H···π mediated (3.732−3.987 Å) porphyrin−porphyrin interactions lead to the formation of a linear array of the dimer that further self-assembles into offset packed 2D layers with voids. Dimer **4** (as observed in **15**), on the other hand, is derived from a linear ligand **4PIN** and displays a perfectly

(16) Moulton, B.; Zaworotko, M. J. *Chem. Rev.* **2001**, *101*, 1629.

(17) (a) Steiner, T.; Starikov, E. B.; Amado, A. M.; Teixeira-Dias, J. J. C. *J. Chem. Soc., Perkin Trans. 2* **1995**, 1321. (b) Cochran, J. E.; Parrott, T. J.; Whitlock, B. J.; Whitiock, H. W. *J. Am. Chem. Soc.* **1992**, *114*, 2269.

linear topology. Thus, it packs the way a linear dimer generally packs (Scheme 2).

The only other two polymers reported thus far (as a result of the CSD search described above) are BABBUC and PIKKID which packed in a fashion wherein the polymers are arranged in parallel arrays displaying no usually observed porphyrin−porphyrin interactions; the adjacent phenyl arms of the porphyrin moieties embrace the axial ligands coming from the neighboring polymeric chains. However, the linear polymeric building **7** found in **18** displays noteworthy packing modes observed thus far in pyridyl-based metallo-TPP polymers. The polymeric units **7** in **18** are packed in a cagelike architecture within which the guest molecules are accommodated.

The hexacoordinated monomeric unit **8** observed in both **19** and **20** displays a unique feature. In both the crystals **19** and **20**, two crystallographically independent monomeric unit **8** are observed in the asymmetric unit. The packing of one type of monomer creates voids within which the other monomeric units along with the guest molecules are accommodated. Such type of packing mode in pyridyl-based hexacoordinated metallo-TPP-based inclusion crystals is, to the best of our knowledge, not reported thus far.

Summary. Pyridyl-based bidentate ligands having various ligating topologies and hydrogen-bonding backbones (amide/urea) have been used to modify ZnTPP/MnTPP building blocks through axial coordination. Thus, single-crystal structures of nine inclusion crystals derived from ZnTPP- or MnTPP-based AMTAMPs generated using axial ligands **4BPU**, **3BPU**, and **4PIN** are reported.

Axial Ligand and AMTAMP Topology. While dimeric AMTAMPs (**1**, **3**, and **4**) are formed in ZnTPP-based materials (**11**, **13**−**15**), the polymeric **7** and hexacoordinated monomeric building block **8** are obtained in MnTPP-based crystals **18** and **19**−**20**, respectively. Pentacoordinated monomeric building blocks **2** and **5** are observed only in ZnTPP-based materials (in **12** and **16**) displaying "board pin" topology. The building block **1** displays a slightly bent topology in **11**. Severely bent topology is also displayed by AMTAMP **3** (as observed in **13** and **14**) which is derived from **3BPU** wherein the pyridyl N atoms are more angularly disposed in its *syn*−*syn* conformation compared to its structural isomer **4BPU**. Meanwhile the amide-based bidentate ligand **4PIN** in which the ligating pyridyl N atoms are linearly disposed results in a linear dimer **4** as observed in **15**. Overall topology of the polymeric building block **7** as observed in **18** is found to be effectively linear although the intra-porphyrin angle is found to be 36.5°. Hexacoordinated monomeric building block **8** as observed in **19** and **20** displays expected topology wherein the axial ligands coordinate to the metal center with the perpendicular approach. However, the axial ligands are protruding out of the porphyrin core in **8** due to the angular disposition of the coordinating pyridyl N atom of the axial ligand **3BPU**.

AMTAMP Topologies, Hydrogen-Bonding Backbone of the Axial Ligand, and Their Influence on the Self-Assembly of the AMTAMPs. The linear dimeric building blocks **1** and **4** as observed in **11** and **15**, respectively, conserve the packing mode of dimeric AMTAMPs. However, the bent AMTAMP **3** as observed in **13** and **14** displays intriguing packing modes not observed thus far. Board pin shaped AMTAMP **2** in **12** does not conserve the packing mode of pentacoordinated monomeric building block; the hydrogen-bonding backbone, namely, urea of **4BPU** influences the self-assembly of the building block involving the hydrogen-bonding interactions of the type N−H···N resulting in a new type of packing. The amide hydrogen-bonding backbone **5** in **16** interacts with the hydrogen bond capable guest 2-*p*-tolylethenol resulting in a supramolecular dimer that packs in a herringbone fashion. It is worth noting that the hydrogen-bonding backbones urea and amide did not show their usual self-complementary hydrogen-bonding interactions[18] in the dimeric building block presumably because of the fact that the hydrogen-bonding functionalities are not sterically accessible for such interactions. Hydrogen-bonding functionalities, however, are able to interact with the hydrogen bonding capable guests. In the MnTPP-based materials, the hydrogen-bonding backbone is mainly interacting with the counterion Cl^- via N−H···Cl interactions.

Porphyrin−Porphyrin Interactions. Porphyrin−porphyrin interactions characterized by C−H···π type interactions involving phenyl arms and pyrrole moieties of the porphyrins are present in all the dimers as observed in the inclusion crystals **11** and **13**−**15** and in pentacoordinated monomers as observed in **12** and **16**. The polymeric building block in **18** and hexacoordinated monomers in **19** and **20** do not show such interactions.

This study clearly demonstrates how the ligating topologies and hydrogen-bonding backbone influences the final supramolecular architectures of the AMTAMPs in the corresponding inclusion crystals. The AMTAMP topology and consequently its supramolecular architecture and inclusion properties can be modulated by choosing appropriate axial ligands. Thus, these results presented here provide further insights into the designing of metalloporphyrin-based inclusion materials.

Experimental Section

Materials and Methods. Syntheses, characterization of ligands **4BPU**, **3BPU**, and **4PIN** were previously reported by our group.[11−12] Monomeric ZnTPP and MnTPP were synthesized according to the standard procedure for porphyrin synthesis. All the solvents were commercially available and used without further purification. FT-IR spectra were recorded using Perkin-Elmer Spectrum GX, and TGA analyses were performed on a Mettler Toledo TGA/SDTA851^e.

AMTAMPs derived from ZnTPP and MnTPP were obtained by reaction of the metalloporphyrins and the corresponding ligands in 1:2 (TAMP:ligand) molar ratio in suitable solvents. Single crystals suitable for X-ray analysis of **12**−**16** (yields 15−20%) and **18**−**20** (yields 40−45%) were obtained by the slow evaporation of these

(18) (a) Hollingsworth, M. D.; Harris, K. D. In *Comprehensive Supramolecular Chemistry*; MacNicol, D. D., Toda, F., Bishop, R., Eds.; Pergamon: Oxford, U.K., 1996; Vol. 6, p 177. (b) MacDonald, J. C.; Whitesides, G. M. *Chem. Rev.* **1994**, *94*, 2383.

solutions. Slow evaporation of a solution of **12** in DMF over a period of 1 week resulted in X-ray-quality single crystals of **11**.

X-ray Diffration. X-ray single-crystal data were collected using Mo Kα ($\lambda = 0.7107$ Å) radiation on a SMART APEX diffractometer equipped with CCD area detector. All the crystals except **15** were isolated from the mother liquor and immediately immersed in Paratone oil and then mounted; a suitable crystal of **15** was sealed in a glass capillary. Data collection, data reduction, and structure solution/refinement were carried out using the software package of SMART APEX. Graphics were generated using MERCURY 1.4.

All structures were solved by direct methods and refined in a routine manner. In most of the cases, non-hydrogen atoms were treated anisotropically. The phenyl rings of the porphyrin moiety were refined as a rigid hexagon in suitable cases. Whenever possible, the hydrogen atoms were located on a difference Fourier map and refined. In other cases, the hydrogen atoms were geometrically fixed.

In **11**, one of the solvent DMF molecules was found to be disordered and was refined with the FVAR second variable facility provided in SHELXL. In **18**, two carbon atoms, C(43) and C(54), of the pyrrole moiety of the porphyrin core were refined isotropically due to high thermal parameters. In **19**, the disordered carbon atom of the guest molecule toluene was refined using the FVAR facility. In all cases, repeated measurements of the unit-cell dimensions from different single crystallites were performed, and the uniform constitution of all AMTAMPs reported herein was confirmed.

Acknowledgment. D. K.K. thanks the CSIR, New Delhi, India, for a senior research fellowship. P.D. thanks the Department of Science and Technology, New Delhi, India, for financial support.

Supporting Information Available: FT-IR data, hydrogen-bonding parameters, TGA plots, and CIFs. This material is available free of charge via the Internet at http://pubs.acs.org.

IC0702163